IJAME
Int. J. of Applied Mechanics and Engineering, 2023, vol.28, No.3, pp.13-27
DOI: 10.59441/ijame/172895

FUZZY LOGIC CONTROL OF ACTIVE SUSPENSION SYSTEM EQUIPPED WITH A HYDRAULIC ACTUATOR

Waleed AL-ASHTARI
Mechanical Engineering Department, College of Engineering, University of Baghdad, IRAQ
E-mail: Waleed.Al.Ashtari@coeng.uobaghdad.edu.iq

In this paper, the Active Suspension System (ASS) of road vehicles was investigated. In addition to the conventional stiffness and damper, the proposed ASS includes a fuzzy controller, a hydraulic actuator, and an LVDT position sensor. Furthermore, this paper presents a nonlinear model describing the operation of the hydraulic actuator as a part of the suspension system. Additionally, the detailed steps of the fuzzy controller design for such a system are introduced. A MATLAB/Simulink model was constructed to study the proposed ASS at different profiles of road irregularities. The results have shown that the proposed ASS has superior performance compared to the conventional Passive Suspension System (PSS), where the body displacement can be minimized to about *70.1* % and the settling time is reduced to about *48.4* %. Also, the results have shown that the actuator force can reach *68* % of the body weight under the worst studied road conditions.

Key words: active suspension system, hydraulic actuator, nonlinear model, LVDT sensor and fuzzy controller.

1. Introduction

In road vehicles, suspension systems are very important components that connect the tires to the body. The main objectives of such systems are reducing the negative effects caused by road irregularities on the vehicle's body, maintaining vehicle stability, and providing comfort to the passengers. The conventional suspension system includes springs and dampers; such a system is known as the Passive Suspension System (PSS). Today, two more suspension systems exist, which are known as the Semi-Active Suspension system (S-ASS) and the active suspension system (ASS). Generally, PSSs are easy to implement and relatively inexpensive. These systems work to dissipate the disturbance energy and reduce its effect on the vehicle's body, depending on the induced friction. Alternatively, S-ASSs were developed in order to improve the vehicle response caused by road irregularities by changing the system stiffness or damping parameters depending on those irregularities. Further development in suspension systems led to the introduction of the ASS. This type of suspension system has its own actuator, which is used to apply force between the vehicle's body and tires in order to achieve the objectives of the suspension system optimally [1].

Hydraulic actuators are widely used on ASSs. This actuator includes mainly a piston, cylinder servo valves, and a supply pump. The operation of the actuator depends on the commands coming from the controller. These commands are calculated based on a certain control algorithm, which considers the information of the road and vehicle statuses in its calculation [2 and 3].

Generally, two adaptive controllers are used in ASS: The Online Self-Tuning Controller (OS-TC) and the Model Reference Adaptive Controller (MRAC). In the OS-TC, the operation of the actuator is continuously adjusted based on certain design rules in order to counter disturbances caused by road irregularities. Alternatively, in the MRAC, a dynamic model describing the response of the suspension system is essentially required. Such a controller works to adapt the system performance based on a certain control algorithm in order to optimize the suspension system response depending on the road conditions [4-6].

However, the MRAC requires a mathematical model for the suspension system. Obtaining a simple linear model describing the response of such a system accurately at different operating conditions is a difficult issue. Actually, the model of a suspension system contains many nonlinearities and uncertainties caused by

the mechanical wear and characteristics of the suspension system elements. Therefore, the OS-TC is intensively used in most published work today [7].

One promising method of the OS-TC used to tackle such nonlinearities and uncertainties in the suspension system is fuzzy logic control. The theoretical studies and experimental work on fuzzy control of suspension systems have shown that fuzzy control can effectively increase the stability of vehicles at any uncertainty. Fuzzy controllers are characterized by low overshoot and strong robustness, as well as their ability to overcome system non-linearities. Unfortunately, this type of controller still requires a larger number of quantization steps to increase the range of rule searching and reduce the decision-making speed in order to adjust the vehicle status efficiently. This attracted the attention of many researchers around the world to introduce new control rules that can compromise the conflict between the accuracy of the control action and its speed in order to achieve the objective of suspension perfectly [8-11].

The fuzzy controller uses fuzzy logic rules to continuously adjust the controlled variables. The controlled variables are calculated depending on the error and the rate of change of that error caused by the road irregularities. There have been a lot of research papers published that study the development of such controllers. Although those studies greatly enhance the accuracy and adaptability of the suspension system controller, this topic still needs more work, especially in the logic rules [12-14].

In the past years, inertial profilers and LIDAR sensors have been used to detect road conditions and obtain real-time information about their irregularities. Although such sensors have highly accurate measurements, the cost of the system sensors is relatively high, and the accuracy is susceptible to the influence of the external environment, such as the weather and road surface condition [15 and 16]. Recently, much of the published work has focused on measuring the road condition based on the response of the suspension system itself, where the response is measured using onboard sensors such as accelerometers or potentiometers [17-20].

This paper presents an ASS that incorporates additional components such as a fuzzy controller, a hydraulic actuator, and an LVDT position sensor in addition to the traditional suspension system elements. The fuzzy controller is utilized to generate the necessary control action based on measurements from the LVDT position sensor, which detects the hydraulic actuator's response to road irregularities. This control action is then applied to the hydraulic actuator to generate the force needed to overcome the road irregularities. The paper also provides a comprehensive functional diagram and nonlinear model for the proposed system, along with a MATLAB/Simulink representation of the derived model.

2. The proposed active suspension system

The functional block diagram of the proposed ASS is shown in Fig.1. The system includes the following elements:

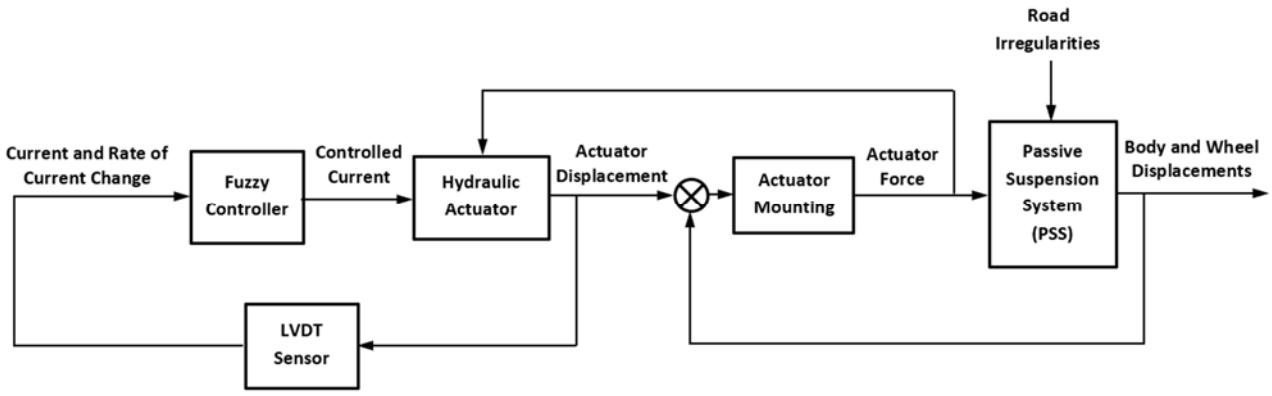

Fig.1. Functional block diagram of the proposed ASS.

1. The fuzzy controller, which used to control the suspension system's operation based on certain designed rules.

2. The hydraulic actuator, which is used to generate the required force for countering the effect of road irregularities on the vehicle response.
3. LVDT sensor, which is used to measure the hydraulic actuator response and provides the required information for the logic controller in order to generate a control action.
4. The actuator mounting, which has a considerable role in the ASS performance.
5. The PSS, which consists of the conventional elements of conventional suspension systems, i.e., the mass of the vehicle body, the mass of the tier, the spring, and the damper.

3. Mathematical modelling

In this section, the mathematical model of each element of the proposed ASS will be introduced.

3.1. Fuzzy controller

The quality of a MRAC's performance is fully based on the accuracy of the dynamic model used in its design. The nonlinear characteristics of the ASS made it even more difficult to define an accurate, simple mathematical model to be used to design such a controller. Furthermore, the mechanical conditions of other elements of the suspension system highly affect the MRAC. Also, the road irregularities cause random noises that mostly cannot be identified. All these cause uncertainties, which can lead to the controller's failure to fulfill its duty. Alternatively, designing a controller based on fuzzy logic theory is one of the most powerful solutions for overcoming such uncertainties. This controller is model-free and has the ability to handle unexpected nonlinearities and situations effectively [21 and 22].

Figure 2 shows the general outline of the proposed fuzzy controller, where $i_p(t)$ is the output current from the LVDT sensor and $i_p(t)$ is the current supplied to the hydraulic actuator. As can be seen from Fig. 2, the main elements of a fuzzy controller are fuzzification, rule base, inference engine, and defuzzification. In such a controller, the fuzzification stage converts the error and the change in error into fuzzy values with the help of the used membership functions. After that, the designed rules are applied according to the selected inference mechanism. Actually, the idea of fuzzy logic is to convert the knowledge of an expert into a control signal with the help of designed rules, where the performance of such a controller depends on the antecedent and consequent parts of the fuzzy rules. Finally, the defuzzification process converts fuzzy values into a command signal applied to the actuator.

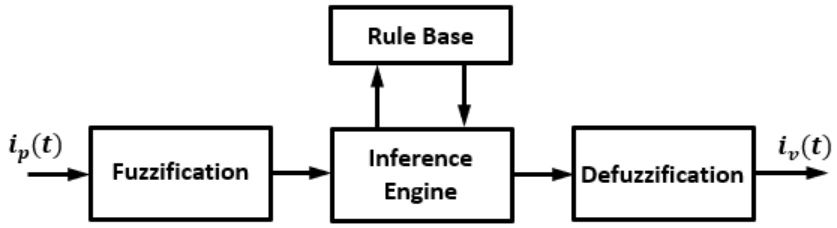

Fig.2. Outline of the proposed fuzzy logic controller

3.2. Active suspension system

In this paper, the quarter-car model shown in Fig.3 was adopted. In this model, $y_b(t)$ is the displacement of the vehicle body, $y_w(t)$ is the displacement of the wheel, and $F_a(t)$ is the force applied by the hydraulic actuator. The governing equation of the vehicle body can be obtained by applying Newton's second law, thus

$$M_b\ddot{y}_b(t)+C\left(\dot{y}_b(t)-\dot{y}_w(t)\right)+K\left(y_b(t)-y_w(t)\right)=F_a(t). \tag{3.1}$$

Also, the governing equation of the wheel can be found by applying Newton's second law, thus

$$M_w\ddot{y}_w(t)+C\left(\dot{y}_w(t)-\dot{y}_b(t)\right)+K\left(y_w(t)-y_b(t)\right)+K_t\left(y_w(t)-y_i(t)\right)=-F_a(t) \tag{3.2}$$

where M_b, M_w, C, K and K_t are denoted as the vehicle body mass, the wheel mass, the damping coefficient of the suspension, the stiffness of the suspension spring, and finally, the stiffness of the tire, respectively.

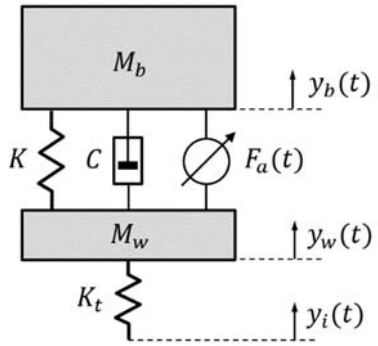

Fig.3. Illustration diagram of the Active Suspension System (ASS).

3.3. Hydraulic actuator

Referring to Fig.4, a hydraulic actuator consists of a piston-cylinder mechanism and a servo valve. The servo valve is responsible for controlling the magnitude and direction of the pressurized hydraulic flow rate that enters the piston-cylinder mechanism. The relationship between the servo valve movement $y_v(t)$ and the servo valve current $i_v(t)$ can be formulated as:

$$\ddot{y}_v(t)+2\zeta_v\omega_v\dot{y}_v(t)+\omega_v^2y_v(t)=k_v\,\omega_v^2\,i_v(t) \tag{3.3}$$

where k_v is the servo gain, ω_v is the servo natural frequency, ζ_v is the servo damping ratio.
The supply flow into the actuator chamber 1 shown in Fig.4 is:

$$Q_{vs}(t)=Q_l(t)+\frac{V_1(t)}{\beta_e}\frac{dP_1(t)}{dt} \tag{3.4}$$

and the return flow from the actuator chamber 2 is:

$$Q_{vr}(t)=Q_l(t)-\frac{V_2(t)}{\beta_e}\frac{dP_2(t)}{dt} \tag{3.5}$$

where $Q_l(t)$ is the flowrate due to load application, $P_1(t)$ is the pressure of chamber 1, $P_2(t)$ is the pressure of chamber 2, and β_e is the effective bulk modulus of the actuator.

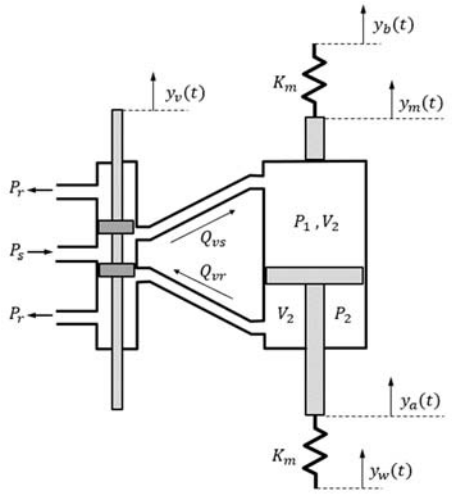

Fig.4. Illustration diagram of the hydraulic actuators: $y(t)$ is the input servo displacement, and $y_a(t)$ is the controlled actuator displacement.

Furthermore, V_1 is the volume of chamber 1, which is given by:

$$V_1(t) = V_o + A_p\, y_a(t) \tag{3.6}$$

and V_2 is the volume of chamber 2, which is expressed as:

$$V_2(t) = V_o - A_p\, y_a(t) \tag{3.7}$$

where V_o is the half volume of the cylinder, A_p is the piston cross-sectional area, and $y_a(t)$ is the actuator displacement. The first terms of Eqs (3.4) and (3.5) are due to the volumetric displacement of the actuator piston, and the second terms are due to fluid compression or expansion in the respective actuator chamber. In the present model, it is assumed that the second terms are equal, i.e.,

$$\frac{V_1(t)}{\beta_e}\frac{dP_1(t)}{dt} = \frac{V_2(t)}{\beta_e}\left(-\frac{dP_2(t)}{dt}\right) = \frac{V_o}{2\beta_e}\frac{dP_l(t)}{dt} \tag{3.8}$$

where $P_l(t)$ is the load pressure, which is given by:

$$P_l(t) = P_1(t) - P_2(t). \tag{3.9}$$

The above assumption leads to.

$$Q_{vs}(t) = Q_{vr}(t) = Q_v(t) \tag{3.10}$$

where $Q_v(t)$ is the valve control flow rate and can be obtained by substituting Eqs. (3.8) and (3.10) into either Eq.(3.4) or Eq.(3.5), which it is found to be;

$$Q_v(t) = Q_l(t) + \frac{V_o}{2\beta_e}\frac{dP_l(t)}{dt}. \tag{3.11}$$

It is extremely difficult to realize a servo valve with ideal characteristics. There will be a finite redial clearance between the servo valve spool land and sleeve, and there will also be either underlap or overlap for the orifice opening. Normally, some overlap will be kept for the orifice opening to reduce the null leakage of the servo valve. Assuming that the radial clearance is C_r and the overlap between spool land and the orifice opening in the sleeve is δ, the effective length of the servo valve orifice $y_o(t)$ caused by the spool displacement of $y_v(t)$ can be approximated to be [23].

$$y_o(t) = y_v(t) - \delta\left[1 - e^{-\left(\frac{\sigma|y_v(t)|}{\delta C_r}\right)}\right] sign\left(y_v(t)\right) \tag{3.12}$$

where σ is a constant. The control flow rate through the servo valve $Q_v(t)$ in terms of the load pressure $P_l(t)$ and the effective length of the servo valve orifice $y_o(t)$ can be expressed as:

$$Q_v(t) = k_{fn}\, y_o(t)\, \sqrt{\left|P_l(t) - \gamma P_s\right|}\; sign\left(P_l(t) - \gamma P_s\right) \tag{3.13}$$

where k_{fn} is the servo valve flow parameter and γ equals to $sign\left(y_v(t)\right)$. By combining Eqs (3.11)-(3.13) with some mathematical manipulations, the following expression can be written [23]:

$$Q_l(t) = k_{fn}\left[y_v(t) - \delta\left(1 - e^{-\left(\frac{\sigma|y_v(t)|}{\delta C_r}\right)}\right) sign\left(y_v(t)\right)\right]\sqrt{\left|P_l(t) - \gamma P_s\right|}\; sign\left(P_l(t) - \gamma P_s\right) - \\ + \frac{V_o}{2\beta_e}\frac{dP_l(t)}{dt}. \tag{3.14}$$

The actuator piston velocity $\dot{y}_a(t)$ can be expressed as:

$$\dot{y}_a(t) = \frac{Q_l(t)}{A_p}. \tag{3.15}$$

3.4. LVDT position sensor

LVDT is used as a position sensor that measures the actuator displacement $y_a(t)$ to provide the fuzzy controller with the required measurements. The LVDT sensor is a second-order system and has the following relationship [24]:

$$\frac{d^2 i_p(t)}{dt^2} + 2\zeta_p \omega_p \frac{di_p(t)}{dt} + \omega_p^2 i_p(t) = k_p \omega_p^2 \, y_a(t) \tag{3.16}$$

where $i_p(t)$ is the output current from the LVDT, k_p is the LVDT sensor sensitivity, ω_p is the LVDT sensor natural frequency, and ζ_p is the LVDT sensor damping ratio.

3.5. Actuator mounting

Referring to Fig.4, $y_m(t)$ is the backward displacement of the actuator mounting bracket, which can be expressed as:

$$y_m(t) = y_a(t) - y_r(t) \tag{3.17}$$

where $y_r(t)$ is the relative displacement between the body and the wheel of the vehicle, which is given by:

$$y_r(t) = y_w(t) - y_b(t). \tag{3.18}$$

Actually, $y_m(t)$ includes all mechanical flexible elements in a cascade with actuator on either side. Assuming K_m is the equivalent stiffness of such elements, then the actuator force can be formulated as:

$$F_a(t) = K_m \, y_m(t). \tag{3.19}$$

4. Case of study

In this section, a case study will be introduced in order to check the performance of the proposed ASS in comparison with the conventional PSS.

4.1. Specifications of the Active Suspension System

The typical parameters of a quarter-car model can be seen in Tab.1. Those parameters were quoted from Mittal and Bhandari [25].

Table 1. Quarter-car specifications.

Description	Symbol	Unit	Value
body mass	M_b	*kg*	*250*
wheel mass	M_w	*kg*	*50*
suspension stiffness	K	N/m	*18600*
suspension damping coefficient	C	$N \cdot s/m$	*1000*
tier stiffness	K_t	N/m	*196000*
mounting stiffness	K_m	N/m	*18600*

Furthermore, the specifications of the used hydraulic actuators can be found in Tab.2. Those specifications are taken from [23].

Table 2. Specifications of hydraulic actuator.

Definition	**Symbol**	**Unit**	**Value**
piston cross sectional area	A_p	m^2	20.44×10^{-4}
damping coefficient	C_a	$N\cdot s/m$	2000
servo valve clearance	C_r	m	0.5×10^{-6}
servo maximum rated current	$I_{v_{max}}$	mA	20
servo valve flow parameter	K_{fn}	$m^3/s\cdot N^{\frac{1}{2}}$	2.386×10^{-4}
sensitivity of servo valve	K_v	m/A	4×10^{-5}
supply pressure	P_s	Pa	2.11×10^{7}
half volume of the cylinder	V_o	m^3	1.063×10^{-4}
effective bulk modulus	β_e	Pa	9.81×10^{4}
servo valve overlap	δ	m	0.5×10^{-6}
overlap parameter	σ	m	0.5×10^{-6}
servo valve natural frequency	ω_v	rad/s	942.48
servo valve damping ratio	ζ_v	-	1

Also, the specifications of the used LVDT sensor can be found in Tab.3.

Table 3. Position sensor specifications (LVDT).

Definition	**Symbol**	**Unit**	**Value**
scale factor	K_p	A/m	202.63
natural frequency	ω_p	rad/s	628.32
damping ratio	ζ_p	-	0.707

4.2. Simulink representation

MATLAB / Simulink was used to construct the block diagram shown in Fig.5, which represents the proposed ASS. As shown in Fig.6, the MATLAB fuzzy logic toolbox was used to learn the fuzzy controller.

Two inputs were selected, which are the current output from the position sensor $i_p(t)$ and its time rate of change. Also, one output was defined, which is the current supplied to the servo valve $i_v(t)$.

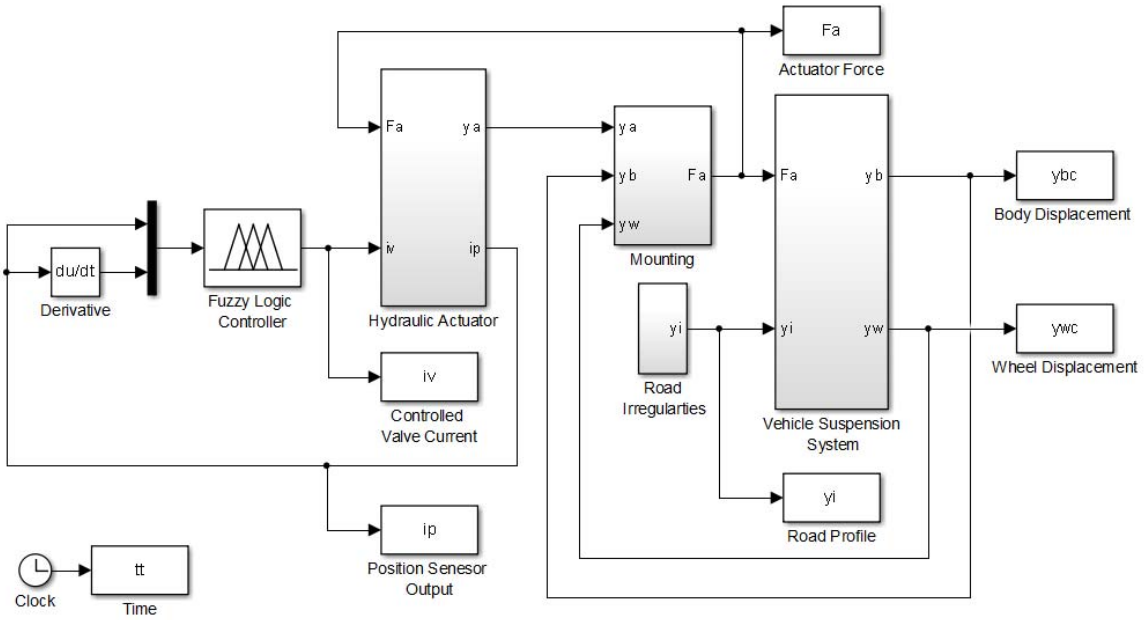

Fig.5. Simulink model of the proposed ASS.

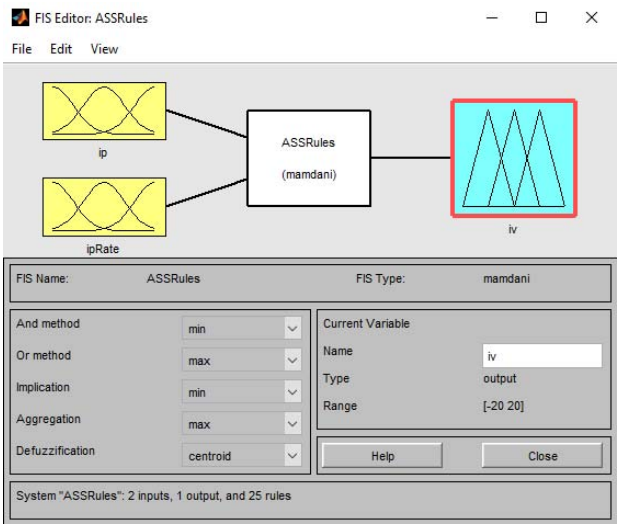

Fig.6. MATLAB / fuzzy logic toolbox representation of the proposed controller.

As shown in Fig.7, a triangular membership function with five linguistic variables was selected to manage the operation of the proposed fuzzy controller. Those variables are NB, NS, ZE, PS, and PB. These abbreviations refer to: Negative Big, Negative Small, Zero, Positive Small, and finally Positive Big, respectively. Figure 7 also shows the range of the inputs and outputs, which were determined depending on the specifications of the used hydraulic actuator and the simulation results at different conditions. These membership functions convert the real input data into fuzzy values in order to reduce the complexity and processing time of the fuzzy controller. Furthermore, a classic interpretation of Mamdani was used as a preference engine.

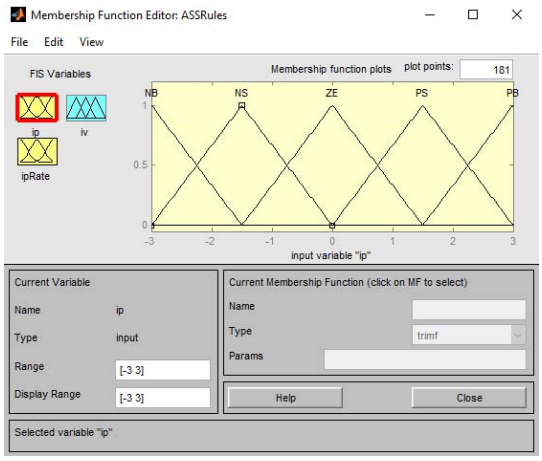

(a) First input $i_p(t)$.

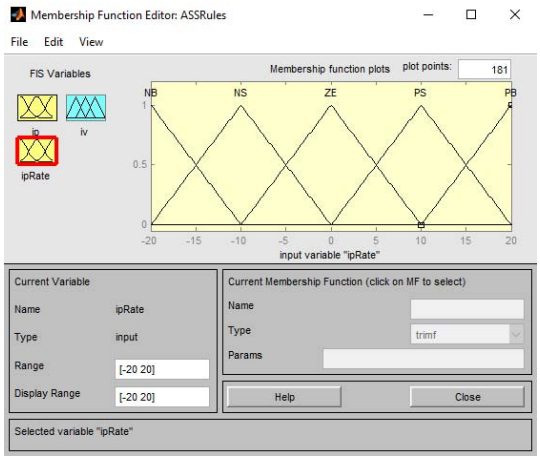

(b) Second input $\frac{di_p(t)}{dt}$.

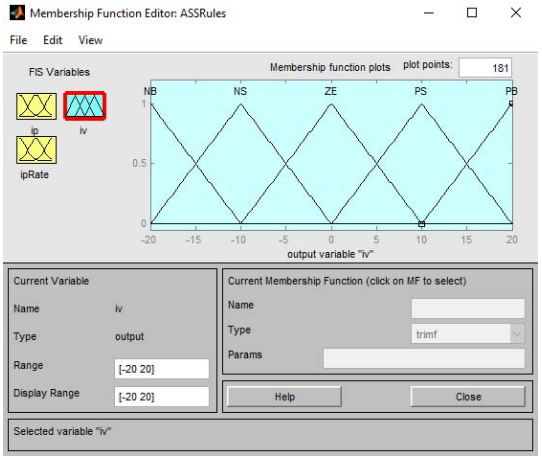

(c) Output $i_v(t)$.

Fig.7. Representation of controller inputs and output with MATLAB / fuzzy logic toolbox.

The proposed rules for the fuzzy logic controller are shown in Tab.4. The fuzzy controller has 25 control rules, which were identified based on the rapidity and effectiveness of the vehicle's body displacement suppression.

Table 4. Fuzzy logic controller rules.

Inputs		$i_p(t)$				
		NB	**NS**	**ZE**	**PS**	**PB**
$\frac{di_p(t)}{dt}$	**NB**	NS	NS	PS	PS	PB
	NS	NS	NS	PS	PB	PB
	ZE	NB	NB	ZE	PB	PB
	PS	NB	NB	NS	PS	PS
	PB	NB	NS	NS	PS	PS
		Output $i_v(t)$				

5. Results and discussion

Three different profiles of road irregularities were investigated. Those profiles are: a single bump, three consecutive bumps, and a cycle of a sine wave. Each of those profiles has an amplitude of *100 mm* and a frequency of *1 Hz*. For each of these road profiles, the body and wheel displacements were calculated for the ASS and the PSS. Furthermore, the controlled current signal and the actuator force of the ASS were determined.

Figure 8a shows the body displacements when the suspension systems were excited by a single bump signal. The figure shows that the ASS has a maximum displacement of about *63.9 mm*, while the PSS has a maximum displacement of about *140.9 mm*. This means that the ASS reduced about *54.6* % of the body displacement. Furthermore, the time that was consumed to settle down the maximum displacement of the ASS and reach *2* % of its maximum value is about *1.41 s*, while the corresponding time for the PSS is about *2.73 s*. Thus, the ASS settling time is about *48.4* % less than that for the PSS. Figure 8b shows the wheel displacement for both investigated systems. It is clear that there is no considerable difference between the two displacements. This could be due to the relatively large magnitude of the tire stiffness. Additionally, Fig.8c shows the output current of the LVDT sensor (uncontrolled) and the current that was supplied to the actuator (controlled). The primary objective of the fuzzy controller is to rapidly mitigate the impact of road irregularities while ensuring that the maximum rated current of the utilized actuator, as defined in the output membership function, is not exceeded. The fuzzy controller is designed with an aggressive approach to swiftly address the effects of road irregularities. In this figure, the maximum current is found to be *16.66 mA*, which is less than the maximum rated current of the used actuator. Finally, Fig.8d shows the force applied by the hydraulic actuator. In this figure, the force was normalized and divided by the weight of the vehicle body, i.e., the actuator force was divided by $M_b \cdot g$, where M_b is the mass of the vehicle body and g is the gravitational acceleration. For a single bump input, the maximum actuator force is found to be about *0.49* times the body weight.

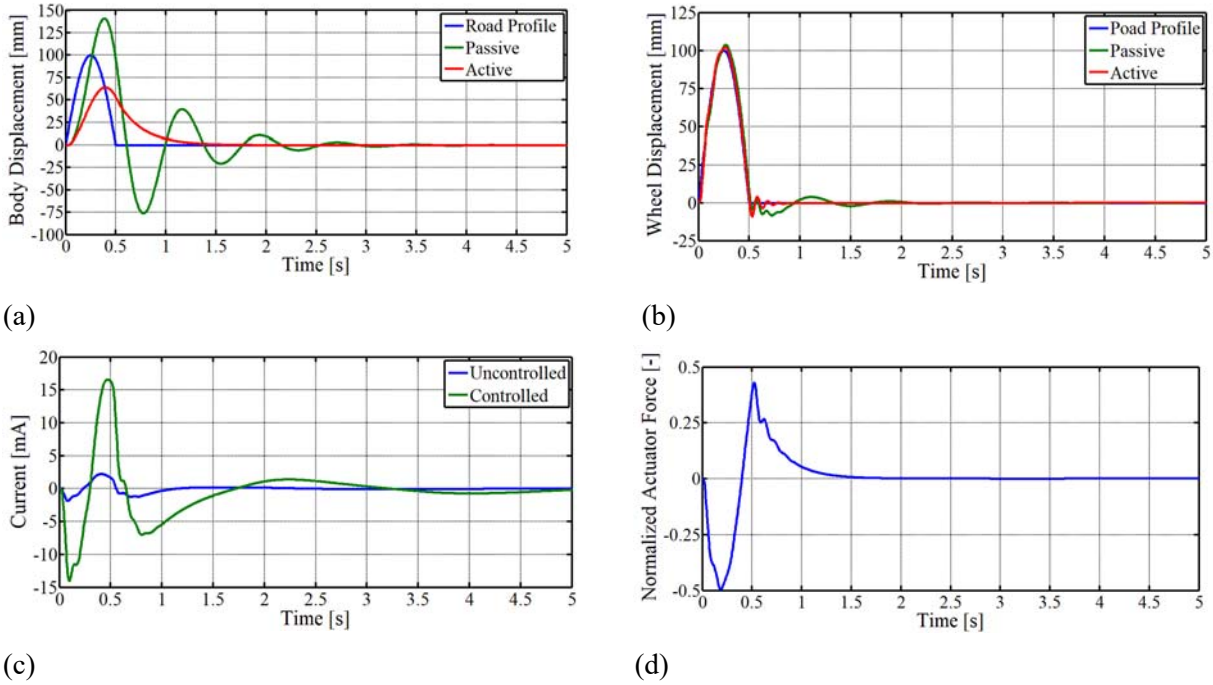

Fig. 8. Responses of the PSS and the ASS to a road profile of single bump.

Going further in the study, the responses of the ASS and PSS to a road profile consisting of three consecutive bumps were investigated. Figure 9a shows a comparison between the body displacements for both the ASS and PSS. It can be seen that the maximum body displacement of the PSS is about *143.9 mm* and the maximum body displacement of the ASS is about *65.3 mm*, which means that there is also about a *54.6* %

reduction in the displacement. Also, Fig.9b shows there is no considerable difference between the wheel displacements of the two systems. The settling time of the PSS is about *4.75 s*, while the corresponding time for the ASS is about *3.40 s*. This means that the ASS requires about *28.4* % less time to settle. Furthermore, Fig.9c shows the uncontrolled and controlled currents, where the maximum required current is about *16.66 mA*. Figure 9d shows the actuator force, which is also found to be *0.49* times the vehicle body weight.

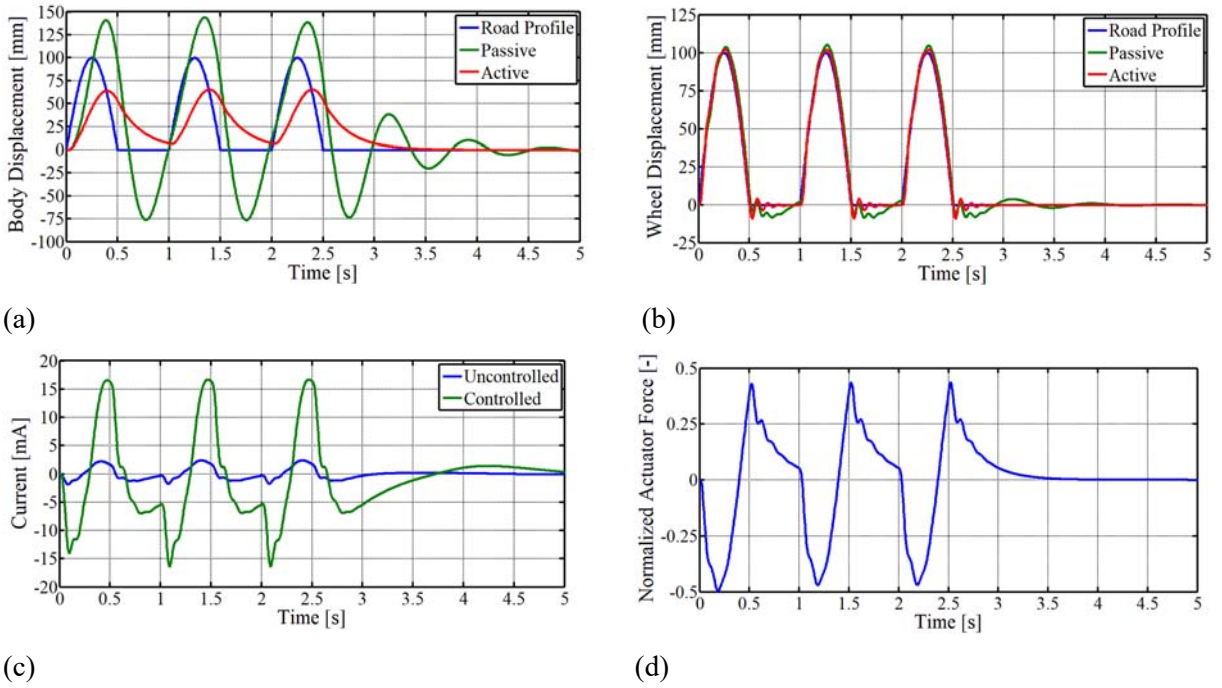

Fig.9. Responses of the PSS and the ASS to a road profile of three consecutive bumps.

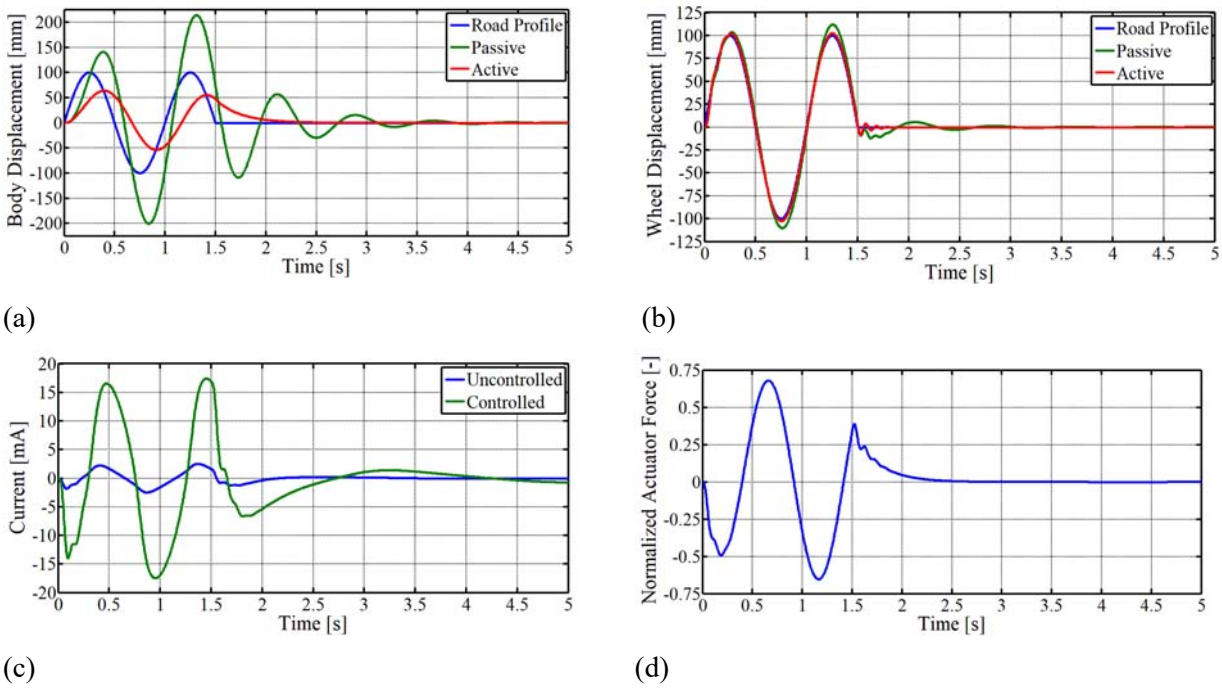

Fig.10. Responses of the PSS and the ASS to a road profile of a one sine wave signal.

Finally, a road profile of a sine wave cycle was investigated. Figure 10a shows the body displacements of the passive and active systems. The figure shows that the maximum displacement of the PSS is about *213.8 mm*, and the corresponding displacement of the ASS is about *63.9 mm*. Therefore, the reduction in body displacement is about *70.1* %. This significant displacement reduction is accompanied by an increase in the controlled current and the actuator force, as shown in Figs 10c and 10d. The maximum controlled current is about *17.44 mA*, and the maximum normalized force is about *0.68*. Also, the wheel displacements show no considerable difference, as indicated in Fig.10b. Furthermore, the settling times of the body displacements are *3.66 s* and *2.38 s* for PSS and ASS, respectively. This means that the ASS has *35.0* % less settling time than the PSS.

From the above results, it is clear that the worst performance of the PSS occurred with the road profile of a cycle sine wave, where the maximum body displacement is about *2.14* times the amplitude of the road profile. In contrast, the ASS shows almost a steady body displacement for the three investigated cases, where the body displacement is about *0.64* times the amplitude of the road profile in all cases. That is because the ASS counters the road irregularities by changing the force applied by the hydraulic actuator. This explains why the maximum normalized actuator force increases to about *0.68* in the cycle sine wave case instead of being *0.49* in the other two cases.

6. Conclusion

In this paper, an ASS including a hydraulic actuator and LVDT sensor is introduced. Furthermore, the proposed ASS is controlled with a fuzzy logic controller. The system was simulated, and the results were obtained using MATLAB and Simulink. The results have shown that the proposed ASS has a better performance compared with the PSS. Briefly, the main results can be summarized in the following points:

1. The body displacement can be reduced to about *70.1* %.
2. The settling time can be minimized to about *48.4* %.
3. The maximum actuator force can be reached at *68* % of the body weight.

Acknowledgement

The author would like to thank all the staff of the Mechanical Engineering Department, College of Engineering, University of Baghdad, for their support and assistance.

Nomenclatures

A_p – piston cross sectional area
C – suspension damping coefficient
C_a – damping coefficient
C_r – servo valve clearance
$F_a(t)$ – actuator force
$I_{v_{max}}$ – servo maximum rated current
$i_p(t)$ – output current from the LVDT
$i_v(t)$ – servo valve current
K – suspension stiffness
K_{fn} – servo valve flow parameter
K_m – mounting stiffness
K_p – scale factor
K_t – tier stiffness
K_v – sensitivity of servo valve
M_b – body mass

M_w – wheel mass
$P_1(t)$ – pressure of chamber 1
$P_2(t)$ – pressure of chamber 2
$P_l(t)$ – load pressure
P_s – supply pressure
$Q_l(t)$ – flow rate due to load application
$Q_v(t)$ – flow rate through the servo valve
$Q_{vr}(t)$ – return flow from the actuator chamber 2
$Q_{vs}(t)$ – supply flow into the actuator chamber 1
V_1 – volume of chamber 1
V_2 – volume of chamber 2
V_o – half volume of the cylinder
$y_a(t)$ – actuator displacement
$y_b(t)$ – body displacement
$y_m(t)$ – actuator mounting bracket displacement
$y_o(t)$ – effective length of servo valve orifice
$y_r(t)$ – relative displacement $y_w(t) - y_b(t)$
$y_v(t)$ – actuator piston displacement
$y_w(t)$ – wheel displacement
β_e – effective bulk modulus
δ – servo valve overlap
σ – overlap parameter
ζ_p – damping ratio
ζ_v – servo valve damping ratio
ω_p – natural frequency
ω_v – servo valve natural frequency

References

[1] Kumar S., Medhavi A. and Kumar R. (2021): *Optimization of nonlinear passive suspension system to minimize road damage for heavy goods vehicle.*– International Journal of Acoustics and Vibrations, vol.26, No.1, pp.56-63.
[2] Tamburrano P., Plummer A.R., Distaso E., and Amirante R. (2018): *A review of electro-hydraulic servovalve research and development.*– International Journal of Fluid Power, pp.1-23.
[3] Lee J., Oh K. and Yi K. (2020): *A novel approach to design and control of an active suspension using linear pump control-based hydraulic system.*– Proceedings of the Institution of Mechanical Engineers, Part D: Journal of Automobile Engineering, vol.234. No.5, pp.1224-1248.
[4] Hua C., Chen J., Li Y. and Li L. (2018): *Adaptive prescribed performance control of half-car active suspension system with unknown dead-zone input.*– Mechanical Systems and Signal Processing, vol.111, pp.135-148.
[5] Ahmed M. and Svaricek F. (2014): *Adaptive anti-windup approach for vehicle semi-active suspension.*– In Proceedings of 2014 International Conference on Modelling, Identification and Control, pp.265-270.
[6] Liu Y.J., Zeng Q., Tong, S., Chen C.P. and Liu L. (2019): *Actuator failure compensation-based adaptive control of active suspension systems with prescribed performance.*– IEEE Transactions on Industrial Electronics, vol.67, No.8, pp.7044-7053.
[7] Han, S. Y., Dong, J. F., Zhou, J., and Chen, Y. H. (2022): *Adaptive fuzzy PID control strategy for vehicle active suspension based on road evaluation.*– Electronics, vol.11, No.6, pp.921.
[8] Na J., Huang Y., Wu X., Su S.F. and Li G. (2019): *Adaptive finite-time fuzzy control of nonlinear active suspension systems with input delay*.– IEEE Transactions on Cybernetics, vol.50, No.6, pp.2639-2650.

[9] Hung N.C., Nhung N.T.B., Vu L.T.Y., Khai V.Q., Son T.A. and Thanh T.Q. (2020): *Apply a fuzzy algorithm to control an active suspension in a quarter car by Matlab's Simulink.*– In Applied Mechanics and Materials, vol.902, pp.23-32.
[10] D'Amato F.J. and Viassolo D.E. (2000): *Fuzzy control for active suspensions.*– Mechatronics, vol.10, No.8, pp.897-920.
[11] Xiang D., Yuan J.Z., and Xu W. (2012): *Study on fuzzy PID algorithm for a new active front steering system.*– Journal of Control Engineering and Technology, vol.2, No.1, pp.24-29.
[12] Han S.Y., Dong J.F., Zhou J. and Chen Y.H. (2022): *Adaptive fuzzy PID control strategy for vehicle active suspension based on road evaluation.*– Electronics, vol.11, No.6, pp.921.
[13] Mahmoodabadi M.J. and Nejadkourki N. (2022): *Optimal fuzzy adaptive robust PID control for an active suspension system.*– Australian Journal of Mechanical Engineering, vol.20, No.3, pp.681-691.
[14] Zhang B., Zhao H. and Zhang X. (2023): *Adaptive variable domain fuzzy PID control strategy based on road excitation for semi-active suspension using CDC shock absorber.*– Journal of Vibration and Control, doi.org/10.1177/10775463231152287
[15] Papadimitrakis M. and Alexandridis A. (2022): *Active vehicle suspension control using road preview model predictive control and radial basis function networks.*– Applied Soft Computing, vol.120, pp.108646.
[16] Lushnikov N. and Lushnikov P. (2017): *Methods of assessment of accuracy of road surface roughness measurement with profilometer.*– Transportation Research Procedia, vol.20, pp.425-429.
[17] Qin Y., Wang Z., Xiang C., Hashemi E., Khajepour A. and Huang Y. (2019): *Speed independent road classification strategy based on vehicle response: Theory and experimental validation.*– Mechanical Systems and Signal Processing, vol.117, pp.653-666.
[18] Dong J.F., Han S.Y., Zhou J., Chen Y.H. and Zhong X.F. (2020): *FNT-based road profile classification in vehicle semi-active suspension system.*– In 2020 IEEE International Conference on Systems, Man, and Cybernetics (SMC), pp. 1392-1397.
[19] Ding R., Wang R., Meng X., Liu W. and Chen L. (2021): *Intelligent switching control of hybrid electromagnetic active suspension based on road identification.*– Mech. Syst. Signal Process, vol.152, pp.107355.
[20] Liu W., Wang R., Ding R., Meng X. and Yang L. (2020): *On-line estimation of road profile in semi-active suspension based on unsprung mass acceleration.*– Mechanical Systems and Signal Processing, vol.135, pp.106370.
[21] Bessa W.M., Dutra M.S. and Kreuzer E. (2022): *Adaptive fuzzy control of electrohydraulic servosystems.*– arXiv, doi.org/10.48550/arXiv.2205.15639
[22] Robert J.J., Kumar P.S., Nair S.T., Moni D.S. and Swarneswar B. (2022): *Fuzzy control of active suspension system based on quarter car model.*– Materials Today: Proceedings, vol.66, pp.902-908.
[23] Kurian P.C., Gopinath A., Shinoy K.S., Santhi P., Sundaramoorthy K., Sebastian B. and Mookiah T. (2017): *Design of servo scheme and drive electronics for the integrated electrohydraulic actuation system of RLV-TD.*– Journal of The Institution of Engineers (India): Series C, vol.98, pp.757-769.
[24] Mandal H., Bera S.K., Saha S., Sadhu P.K. and Bera S.C. (2018): *Study of a modified LVDT type displacement transducer with unlimited range.*– IEEE Sensors Journal, vol.18, No.23, pp.9501-9514.
[25] Mittal R. and Bhandari M. (2015, April): *Design of robust PI controller for vehicle active suspension system with hydraulic actuator.*– In 2015 International Conference on Communications and Signal Processing (ICCSP), pp.0914-0918.

Received: April 5, 2023
Revised: July 28, 2023